Islamic Azad University

Journal of
Optoelectronical Nanostructures

Summer 2024 / Vol. 9, No. 3

Research Paper

A Printed Circuit Board Metamaterial for H9N2 Avian Flu Virus Sensing Based on Plasmonic Induced Transparency in THz Regime

Abdolrasoul Gharaati[*,1], Mohammad Reza Forouzeshfard[2], Maryam Salari[1]

[1]Department of Physics, Payame Noor University, Tehran, Iran
[2]Department of Physics, Vali-e-Asr University, Rafsanjan, Iran

Received: 27 Feb. 2024
Revised: 13 Mar. 2024
Accepted: 1 Jun. 2024
Published: 15 Sep. 2024

Keywords:
Plasmonic induced transparency, Double Split Ring Resonators (DSRRs), Printed Circuit Board, Sensor, Avian flu virus

Abstract

In this article, plasmonic induced transparency (PIT) in a structure consisting of a hybrid split ring resonator has been investigated and researched using computer simulation. One of the most important advantages of the structure is its design based on availability and cheapness Printed Circuit Boards (PCBs) and operation on the THz regime as well. Internal rotation Split Ring Resonators (SRRs) create the PIT effect on the structure by breaking the angular symmetry of the inner ring while the outer ring is fixed. In this article, change in different parameters including the inner and outer radius of the rings, the width of the rings, the gap size, the distance between the left and right rings and the thickness of the substrate have been investigated and the effect of each on improving the transparency of plasmonic induction has been reported. It is shown that the structure can be introduced as a refractive index sensor. Some sensitivity of 240GHz/RIU is reported for the structure. The structure has also been shown to be a good candidate for the detection of H9N2 avian influenza virus.

Citation: Abdolrasoul Gharaati, Mohammad Reza Forouzeshfard, Maryam Salari A Printed Circuit Board metamaterial for H9N2 avian flu virus sensing based on plasmonic induced transparency in THz regime. **Journal of Optoelectronical Nanostructures. 2024; 9 (3): 33-52. DOI: 10.30495/JOPN.2024.32973.1310**

***Corresponding author**: Abdolrasoul Gharaati
Address: Department of Physics, Payame Noor University, Tehran, Iran.
Tell: 00989173135842 **Email:** agharaati@pnu.ac.ir

1. INTRODUCTION

Biological applications of terahertz waves involve studying the properties of biomolecules, cells, and tissues. Terahertz imaging techniques can provide detailed information about the structural and chemical composition of biological samples. This has implications in biomedical research, cancer detection, and pharmaceutical development. Moreover, terahertz waves offer non-invasive imaging capabilities, minimizing potential harm to living organisms [1]. The presence of numerous intra/intermolecular vibration modes in biomaterials like proteins and DNA within the terahertz (THz) spectral range has sparked significant interest in utilizing THz spectroscopy for biomaterial research. One key advantage of THz spectroscopy, in contrast to other optical techniques such as ultraviolet or X-rays, is its non-invasive and non-ionizing nature. This characteristic enables THz spectroscopy to be employed as a spectroscopic tool for analyzing even more complex structural biomaterials, including cells and tissues, without concerns about thermal fluctuations or other nonlinear side effects .In proteins, conformational information is of great importance for understanding molecular interactions and binding with ligands. THz spectroscopy has the potential to analyze these conformational changes, as the energy associated with protein-ligand binding falls within the THz range. However, the detection of small changes in optical properties using conventional THz spectroscopic systems can be limited due to the small absorption cross-section of biomaterials in the THz range [2]. Recently, there have been developments in metamaterial sensing chip-based terahertz (THz) detection techniques that offer highly sensitive and selective detection of carbohydrates. Metamaterials are artificially engineered materials with unique electromagnetic properties that can manipulate and control the interaction of THz waves with matter [2].

Metamaterials [3-5], with their controllable electromagnetic properties, have indeed shown great potential in the highly sensitive and label-free detection of biomolecules [6, 7], These engineered materials have opened up new possibilities for detecting minuscule quantities of various biomolecules [2], including proteins [8], sugars [9], viruses [8, 10-13]. The ability of metamaterials to generate surface plasmons and enhance localized electric fields makes them highly suitable for sensing applications [14-17]. This unique combination of properties intensifies the interaction between light and matter, enabling the highly sensitive detection of even subtle environmental changes [1].

Metamaterials, with their engineered electromagnetic properties, offer a platform for replicating and harnessing the principles of EIT in a broader range of frequencies and scales [16-21]. By designing the structure and composition of metamaterials, researchers can create artificial systems that exhibit similar characteristics to those observed in atomic and condensed matter systems. EIT is a quantum phenomenon that occurs when a pump laser excites the dark state of a system in a specific manner, resulting in the creation of a transparency window within a broader bright state. The pump laser is carefully tuned to interact with the system, causing the dark state to become resonantly coupled with the bright state. EIT has been observed in different media such as cold atoms, warm atoms, and plasmas. However, the practical implementation of EIT has been challenging due to the demanding experimental conditions involved. Since the initial demonstration of EIT in metamaterials, referred to as plasmon-induced transparency (PIT), researchers have proposed various types of metamaterial structures for achieving PIT effects. These structures are designed to manipulate the interaction between electromagnetic waves and resonant elements within the metamaterial, replicating the behavior of EIT [1, 2, 4, 9, 10, 22, 23].

In the PIT phenomenon, dark-bright or bright-bright plasmonic antennas can create induced transparency through interaction [3, 15, 24, 25]. The dark antenna has no interaction with the radiated light lonely, but when it is placed in the vicinity of the bright antenna, the near field of the bright antenna excites the dark antenna and induced transparency occurs.

Surface plasmons, which are collective electron oscillations at the interface between a metamaterial and the surrounding medium, are indeed sensitive to changes in the refractive index of the environment [26]. Indeed, the sensitivity of surface plasmons to changes in the refractive index of the environment has been extensively utilized as a powerful tool for optical sensing. This phenomenon forms the basis of various optical sensing techniques and devices. Plasmonic structures in sensor design offer enhanced sensitivity to refractive index changes, providing a label-free detection method without the need for chromophore labeling. This advancement in plasmon-based sensors has addressed the limitations of conventional optical sensors, resulting in improved sensitivity, optical stability, tunability, and usability in various environments, including living systems [27-29].

One of the most significant applications of metamaterial sensors is in the biomedical field. For example, such sensors can be used for cancer cell detections, health care applications [30-35], blood component [36] and virus measurements [8, 10-12, 27].

Avian influenza (AI), also known as bird flu, is a potentially variable disease

caused by type A influenza viruses. The natural hosts and reservoirs of these viruses are wild aquatic birds, such as ducks and shorebirds, where infections typically do not cause apparent illness (asymptomatic) [10].

The detection and identification of viruses are crucial in understanding and combating severe diseases such as influenza A (H1N1), foodborne illnesses, and Middle East respiratory syndrome (MERS). Traditional detection techniques can be time-consuming and labor-intensive, necessitating the exploration of alternative methods [10].

In this article, by using a metamaterial structure based on double split ring resonators deposited on available and cheap Printed Circuit Board (PCB), first, the phenomenon of induced transparency is investigated and then the application of this metamaterial is investigated in the detection of three types of avian influenza (AI) virus.

2. STRUCTURE

The 3D view and geometric parameters of the proposed structure are shown in Fig. 1. This structure uses a pair of double split ring resonators (DSRRs) made of copper (ε=5.96×107 S/m, μ=1). These DSRRs are placed on a PCB Rogers RT5880 substrate (ε=2.2, tanδ=0.0021) so that the large rings in the DSRRs are fixed and mirror images of each other, while the small SRRs rotate around their center axes. The simulation was done in computer simulation technology (CST) software with unit cell boundary conditions along the X and Y directions. The electromagnetic wave is incident in Z direction, normal to the structure. The electrical field is in X direction.

In the proposed structure, the pair of inner (outer) rings play the role of a dark (bright) antenna. This means that this antenna does not directly interact with the incident light. This is shown in Figs 2-a and 2-b and in Fig.3, as well. The combination of dark and bright antenna and after counterclockwise rotating of the inner rings the symmetry can break and cause to observe induced transparency.

If we place the SRRs in close proximity to each other, the dark antenna is able to indirectly interact with the incident light using the near field of the bright antenna. In fact, the dark mode is paired with the bright mode, and this pairing leads to excite the dark mode. Therefore, the proposed unit cell contains two resonant modes, dark and bright (Fig. 2), and the spectral response of the PIT effect is caused by the destructive interference between these two modes. The PIT effect in this nanostructure occurs when the rings rotate.

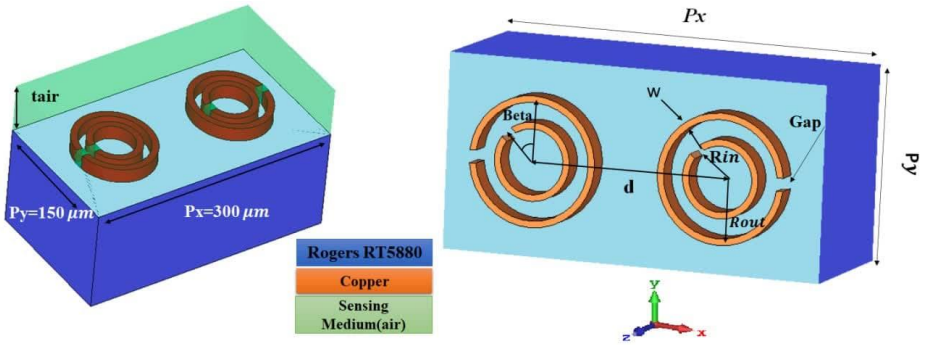

Fig. 1. 3D schematics view of the proposed structure with the parameters of Rin=27μm, Rout=46μm, Px=300μm, Py=150μm, w=7.5μm، d=75μm, Gap=10μm tRogers=252μm, tcu=35μm

3. PLASMONIC INDUCED TRANSPARENCY

Counter clockwise rotation of the inner rings can break the symmetry and cause to have induced transparency. The β angle is the angle between the Y-axis and the inner ring gap as shown in Fig. 1. At the angle β=0, the magnetic fields are symmetric and in opposite directions. thus, no induced transparency is observed, which can be seen in Fig. 2-b. By changing the angle β from 0 to 90, the symmetry is lost and transparency will be visible according to Fig. 2.

Fig. 3 shows the transmission diagram of bright and dark modes individually, as well as their combination at two different angles β=0 and β=90 degrees. The figure clearly shows the dark and bright nature of the modes and plasmonic induced transparency phenomenon at the frequency of 0.4THz for β=90. In this frequency, the graph corresponding to β=0 has an approximate transmission rate, equal to zero, and in the graph β=90, the transmission rate is 0.71, which indeed describes the induced transparency.

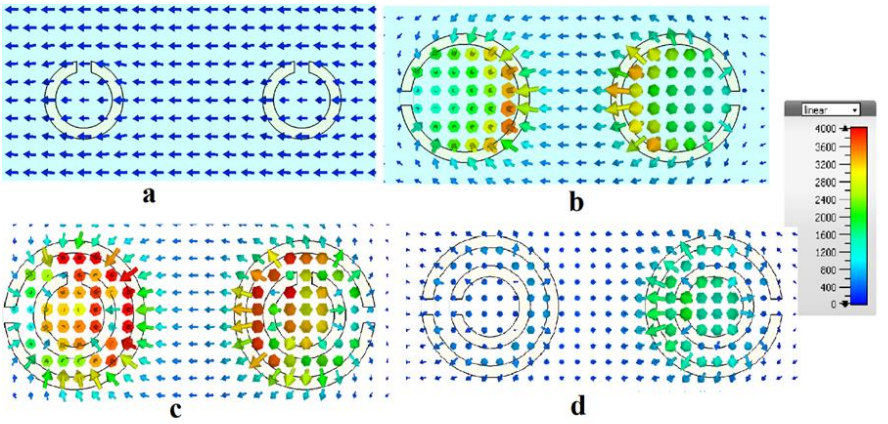

Fig. 2. Distribution of magnetic fields related to (a) dark (b) bright (c) combination of dark and bright antennas at angle β=0, (d) β=90 at 0.4 THz frequency.

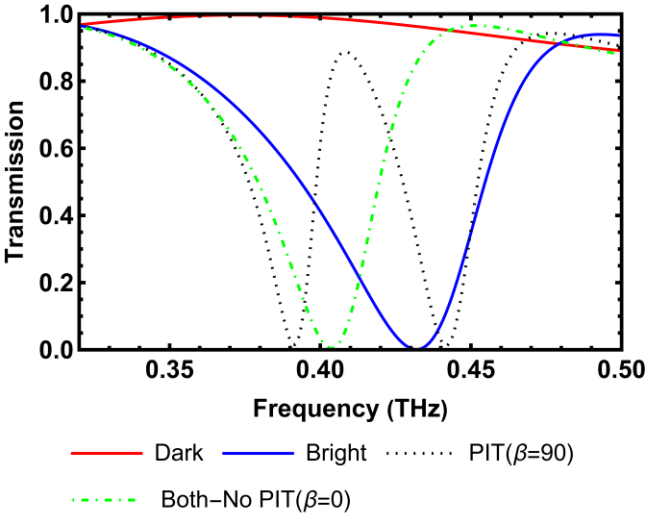

Fig. 3. Transmission spectrum in the presence of bright antenna (blue), dark antenna (red) dark and bright antennas at the same time at β=90 (brown dotted) and at β=0 (green dash-dotted).

Different stages of geometrical symmetry breaking are shown in Fig. 4. At the angle β=0 according to Fig. 2-C, the magnetic fields are symmetric and opposite to each other, so they neutralize each other, and therefore the PIT is not observed. At the angle β=90 according to Fig. 2-D, the magnetic fields are not symmetrical and cannot cancel each other out, so complete destructive interference does not occur, and the PIT is observed.

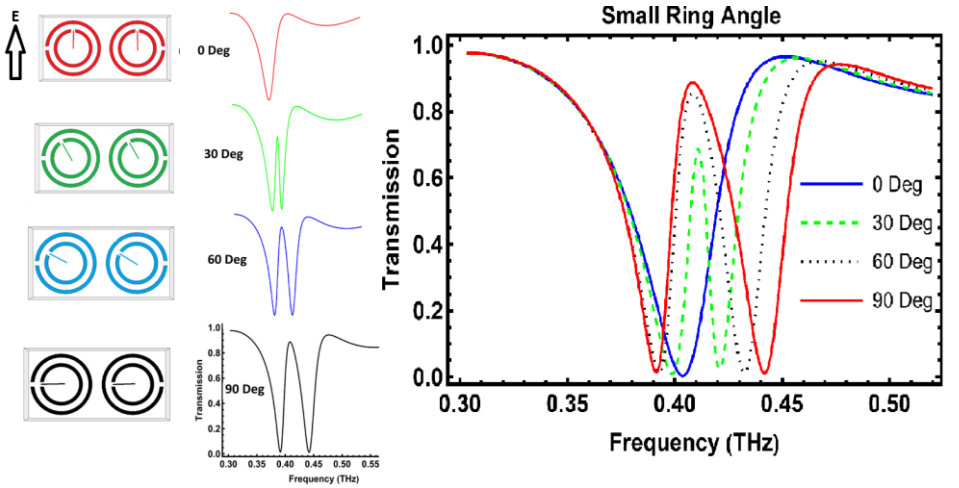

Fig. 4. Transmission spectrum for different stages of symmetry breaking at angle β=0 to β=90.

4. TUNABILITY OF THE STRUCTURE

In order to change and adjust the operating frequency of the device and investigate the effect of the material and geometrical size of the structure, it is necessary to analyze the effect of changing these parameters in the transmission diagram. It is good to noticed that, in explaining the reason for frequency shift in transmission diagrams, it is customary to introduce an equated LC circuit for the structure. The resonance frequency of this circuit is obtained from the relation (1) [25]

$$f = 2\pi \frac{1}{\sqrt{LC}}, \qquad (1)$$

where L is the effective inductance coefficient and C is the effective capacitance of the equivalent circuit. In the following, we will use this relation in explaining the changes in some diagrams.

A. Changing the material of the substrate

By changing the sub-layer with different dielectric constant, the best possible state between the sub-layers was investigated, with the priority to have a better induction transparency and a symmetrical diagram at the β=90 angle. The meaning of better PIT is that the frequency of transparency at the PIT peak at the angle β=90 and the frequency of darkness at the dip β=0 be closer to each other. The higher value of difference in the transmission between the dip and

the peak the better PIT effect. It can be seen in Fig. 5 that the substrate with a lower dielectric constant has created a better induction transparency, so Rogers RT5880 PCB is used to continue the investigation.

TABLE I

PHYSICAL PROPERTIES OF THE DIFFERENT PCB FOR SUBSTRATE.

substrate	Epsilon	Mu	Electric tanδ
Rogers RT5880	2.22	1	0.0021
Rogers RT5870	2.33	1	0.0012
FR-4	4.5	1	0.025
Rogers RO3006	6.5	1	0.002

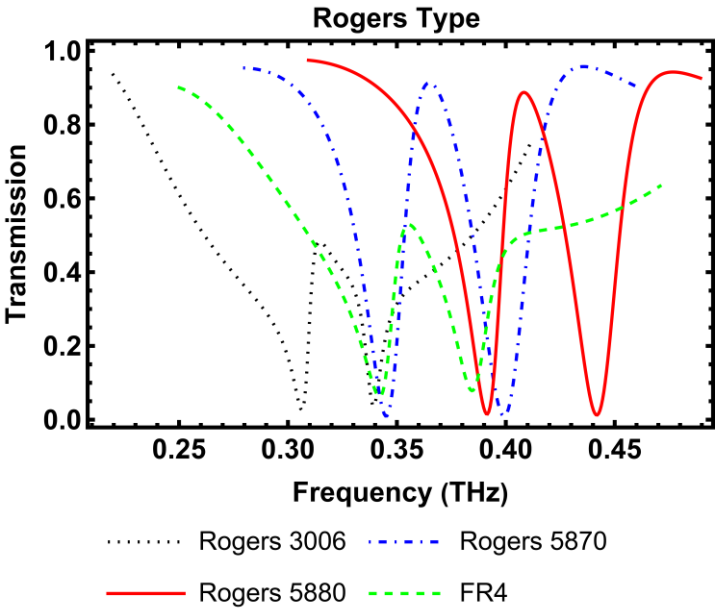

Fig. 5. Transmission spectrum by changing the material of the substrate.

B. Change in copper thickness

Two different thicknesses of copper available in the market, 18 and 35μm, were examined in Fig. 6, considering that better induced transparency is obtained for the thickness of 35μm, so, this thickness is used. Increasing the copper thickness

causes an increase in the area of the capacitor plates formed in the gaps, and as a result, the capacitance increases, and therefore, according to equation (1), the resonance frequency decreases.

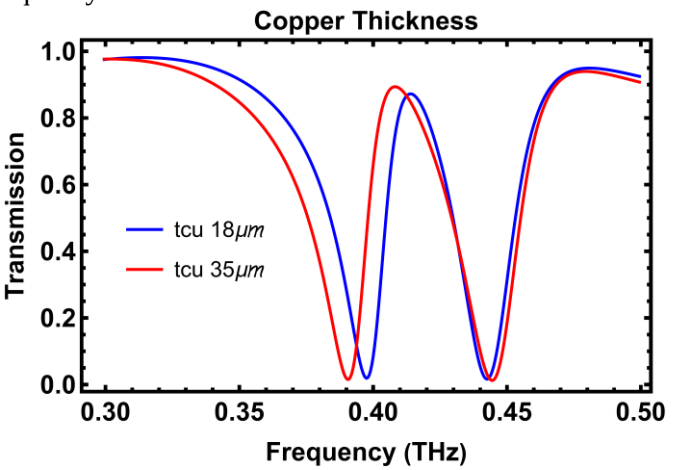

Fig. 6. Transmission spectrum by changing the thickness of copper rings.

C. Change the thickness of the sub layer

Considering some commercially available thicknesses for the Rogers RT5880 substrate in Fig. 7, due to better transparency, 252μm thickness has found to be more suitable.

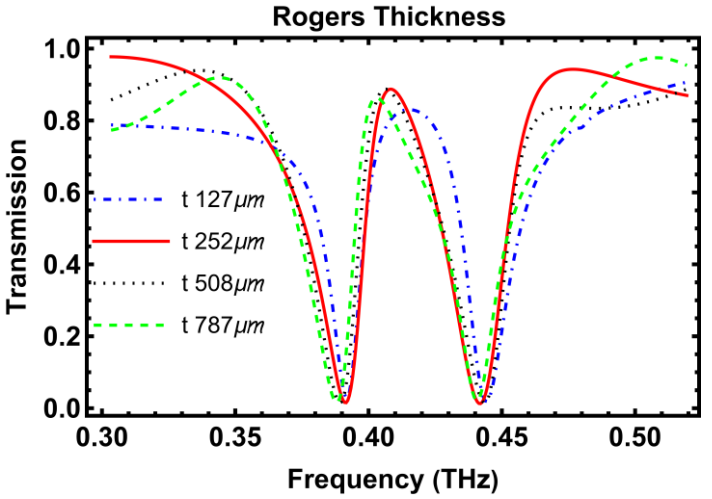

Fig. 7. Transmission spectrum by changing the thickness of the substrate.

D. Changing the internal and external radius

By changing the radius of small and large copper rings, their effect on transparency has been investigated by Fig. 8. Here, the radial distance between two rings is considered to be fixed (19µm) and by examining different radii in order to achieve better induction transparency, the inner and outer radii of 27µm and 46µm were selected for inner and outer radius, respectively. As it is clear from Fig.8, the increase in the radius of the rings leads to shift of the diagram towards lower frequencies, which can be attributed to the increase of the inductance coefficient L in the equivalent circuit due to the increase in the area of the rings. Changing the radius of just inner rings individually will lead to the shift of the left dip.

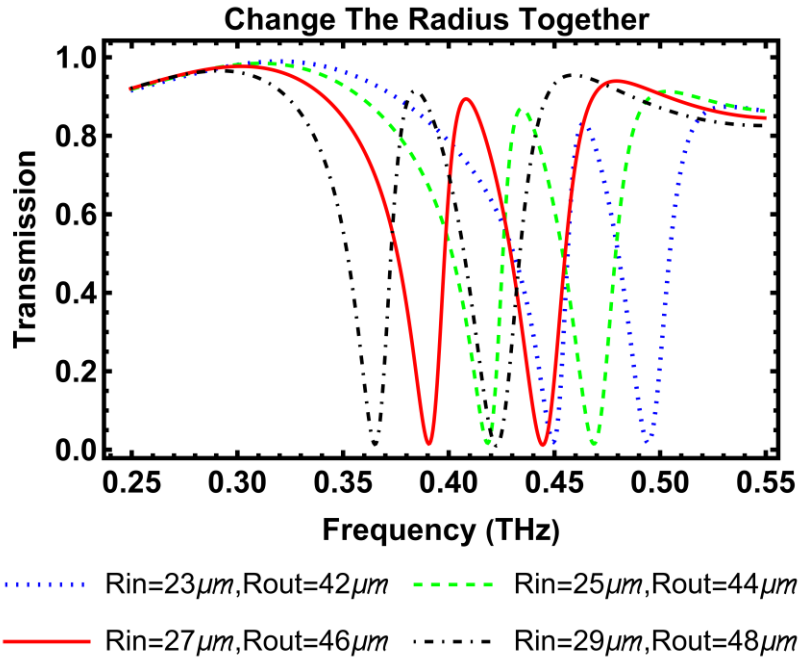

Fig. 8. Transmission spectrum by changing the radius of the rings.

E. Change the distance between the two centers of the rings d

The distance between the two centers of the left and right rings, d, its value was changed between 65µm and 95µm. According to the position of the resonance frequency at the angles of 0 and 90 degrees, the value of 75µm was more suitable for d. Increasing the distance between pair of rings causes a weaker

interaction between them and lead to have a shorter transparency peak, which is clearly visible in Fig. 9.

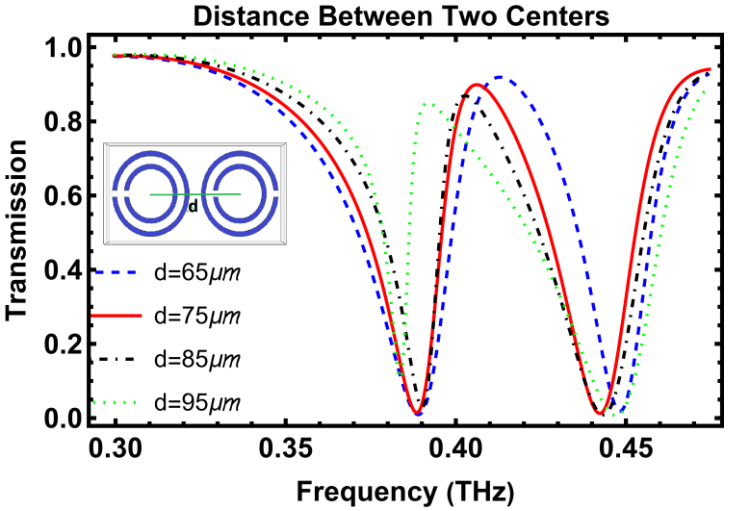

Fig. 9. Transmission spectrum by changing the distance of the rings

F. Changing the width of rings W

By examining the effect of ring width on transparency, it is observed that, a blue shift is generally occurs as a result of increasing the width of the rings in the curve. Also, the symmetry of the chart is disrupted from 9.5μm onwards. As a result, 7.5μm width was selected for subsequent calculations.

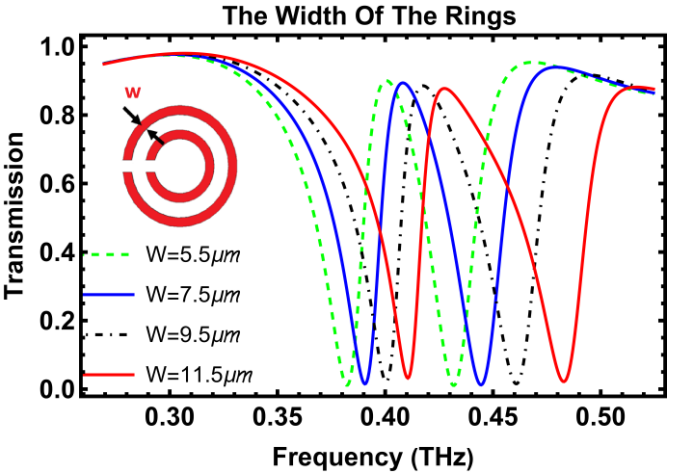

Fig. 10. Transmission spectrum by changing the width of the rings.

G. gap width

Increase the width of the gap causes the decrease in capacitance of capacitor formed in the gap and therefore increases the frequency of resonance according to the equation (1), which can be observed in Fig. 11.

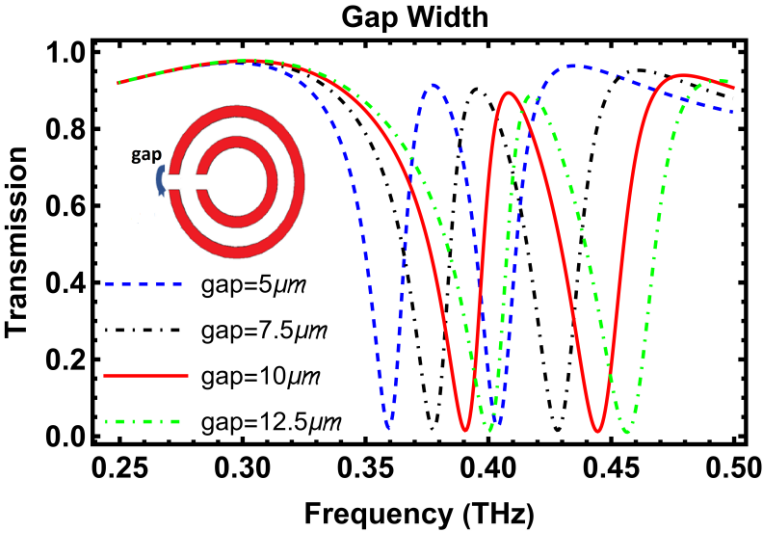

Fig. 11. Transmission spectrum by changing the width of the gap

5. APPLICATIONS

A. Refractive index sensor

For analyzing the feasibility of the structure to be as a sensor, the sensitivity in changing the environment medium is studied. The environment refractive index is changed from n=1 for air to 1.5 by steps of 0.1 and each time the transmission diagram is shown in Fig. 12. The sensitivity is calculated according to the equation of $S = \Delta f/\Delta n$. Therefore, if the line diagram of resonance frequency versus of refractive index is drawn, the slope of the diagram will indicate the sensitivity value.

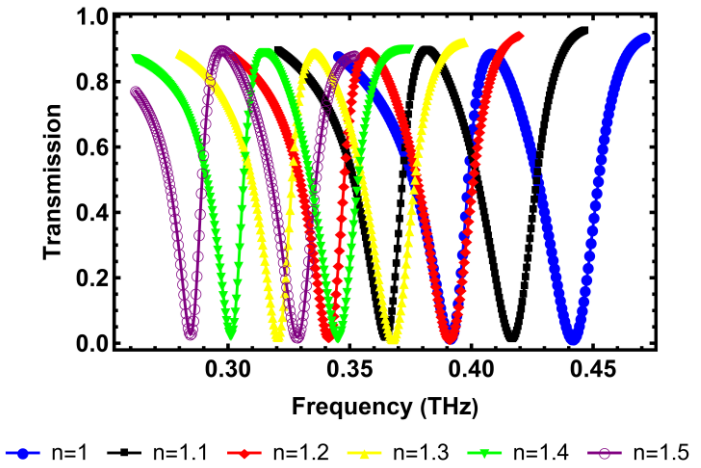

Fig. 12. Transmission spectra by changing the refractive index of the sensing medium from n = 1 (air) to n = 1.5 for the structure of Fig. 1

The maximum sensitivity of the graphs according to Fig. 13 is obtained as 240GHz/RIU which for right dip and PIT peak as well.

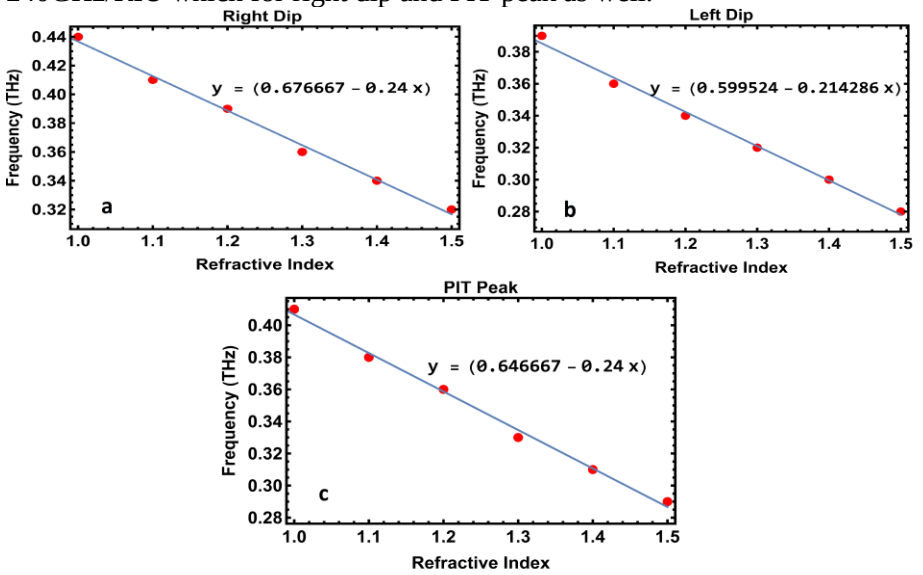

Fig. 13. Resonance frequency location for (a) right depth (b) left dip (c) PIT peak. With changing in refractive index of sensing medium. The slope of the graph indicates the sensitivity, whose value is (a) 240 GHz/RIU for the right dip (b) 214 GHz/RIU for the left dip (c) 240 GHz/RIU for the PIT peak.

B. Influenza virus detection sensor

As an application for this structure, we investigate the capability of the structure for detecting of AI virus, including three subtypes H1N1, H5N2, H9N2.
These three viruses have different refractive indices, which are their distinguishing features. Table II shows their mixed refractive indices at a certain concentration [2].

TABLE II
REFRACTIVE INDEX OF THREE TYPES OF AVIAN FLU VIRUSES. [2]

Subtype-strain name	complex refractive indices	Total protein concentration (mg/ml)
A/NWS/33 (H1N1)	$N = n + 1.4ik$	0.54
A/wild bird/Korea/K09-652/2009 (H5N2)	$N = n + ik$	0.2
A/Korean native chicken/Korea/ k040110/2010 (H9N2)	$N = 1.2n + 1.4ik$	0.28

n and k in Table II are the real and imaginary parts of the refractive index, and its value is obtained from the equation (2) with constant values of γ=4.0, ω_p=4.0THz, ω_0=2.8π THz [10]

$$\varepsilon = 1.5^2 - \frac{\omega_p{}^2}{(\omega^2 - \omega_0{}^2 + i\gamma\omega)} . \qquad (2)$$

By adding a virus layer to the structure instead of the air layer (sensing medium) in Fig. 1, the transmission diagrams for different viruses were drawn in Fig. 14. According to the diagram, it can be claimed that this structure can be a suitable sensor to distinguish H9N2 from other two viruses.

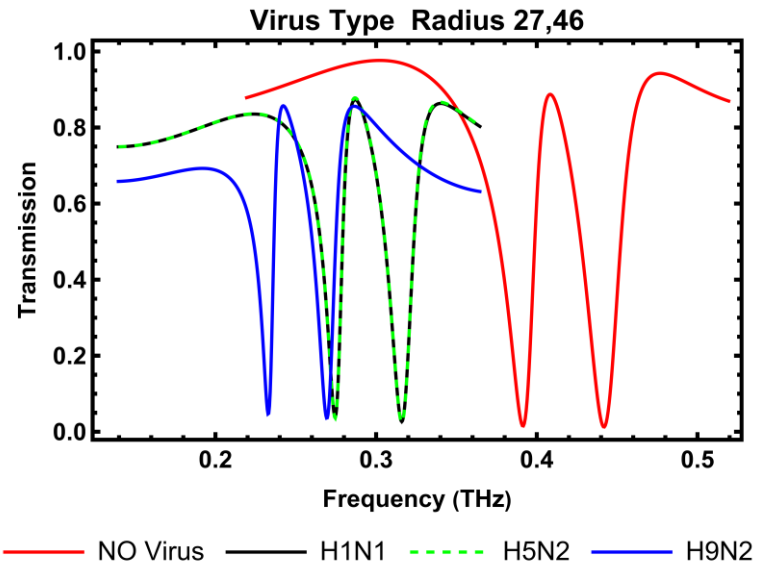

Fig.14. Transmission spectra in the presence of different types of bird flu virus.

6. CONCLUSION

A designed structure composed of available commercial PCB structure is analyzed to have PIT response in transmission diagram in THz regime. The structure is composed of a pair of hybridized SRR and the PIT effect is observed when the inner rings of SRR rotate around its center. It is observed that the transmission spectra of the structure are changed when some physical/geometrical properties of the structure are changed. It is observed that a blue shift is observed in the transmission diagram when the gap size and the ring thickness are increased; There is also a red shift in the transmission diagram when the ring radius and the distance between the rings are increased. An equated LC circuit analyses is introduced for explaining some changes in diagrams. It is also showed that, the structure is able to have sensor capability for refractive index change of environment medium. At the end, we showed that the structure is a good candidate for H9N2 AI Influenzas virus.

REFERENCES

[1] M. Guan, et al. *High-Sensitivity Terahertz Biosensor Based on Plasmon-Induced Transparency Metamaterials*. in Photonics. (2023) MDPI. available online: https://www.mdpi.com/2304-6732/10/11/1258

[2] D-K. Lee, et al., *Nano metamaterials for ultrasensitive Terahertz biosensing.* Scientific reports, (2017). 7(1): p. 8146. available online:

https://www.nature.com/articles/s41598-017-08508-7

[3] W. Cai, and V.M. Shalaev, *Optical metamaterials*. Vol. 10. (2010 Springer. available online:

https://pubs.aip.org/physicstoday/article/63/9/57/386596/Optical-Metamaterials-Fundamentals

[4] M. Parvinnezhad Hokmabadi, et al., *Plasmon-induced transparency by hybridizing concentric-twisted double split ring resonators.* Scientific reports, (2015) 5(1): p. 15735. available online:

https://www.nature.com/articles/srep15735

[5] M. Amin, O. Siddiqui, and M. Farhat, *Linear and circular dichroism in graphene-based reflectors for polarization control.* Physical Review Applied, (2020) 13(2): p. 024046. available online:

https://journals.aps.org/prapplied/abstract/10.1103/PhysRevApplied.13.024046

[6] M.R. Forouzeshfard, and M.H. Farzad, *Electromagnetic wave propagation through two coaxial transformation-based cylindrical media.* Plasmonics, (2015) 10: p. 1345-1357. available online:

https://link.springer.com/article/10.1007/s11468-015-9935-0

[7] E. Moghbeli, H. Askari, and M. Forouzeshfard, *Analyzing the effect of geometric parameters of double split ring resonator on the effective permeability and designing a cloak of invisibility in microwave regime.* Applied Physics A, (2018) 124(5): p. 361. available online:

https://link.springer.com/article/10.1007/s00339-018-1774-3

[8] Q. Niu, R. Zhang, and Y. Yang, *High sensitivity and label-free detection of the SARS-CoV-2 S1 protein using a terahertz meta-biosensor*. Frontiers in Physics, (2022) 10: p. 859924. available online:

https://www.frontiersin.org/articles/10.3389/fphy.2022.859924/full

[9] M.R. Forouzeshfard, S. Ghafari, and Z. Vafapour, *Solute concentration sensing in two aqueous solution using an optical metamaterial sensor.* Journal of Luminescence, (2021) 230: p. 117734. available online:

https://www.sciencedirect.com/science/article/abs/pii/S0022231320317014

[10] A.Keshavarz, and Z. Vafapour, *Sensing avian influenza viruses using terahertz metamaterial reflector.* IEEE Sensors Journal,(2019) 19(13): p. 5161-5166. available online: https://ieeexplore.ieee.org/abstract/document/8663385

[11] S. Park, et al., *Sensing viruses using terahertz nano-gap metamaterials.* Biomedical optics express, (2017) 8(8): p. 3551-3558. available online:

https://opg.optica.org/boe/fulltext.cfm?uri=boe-8-8-3551&id=369089

[12] M. Amin, et al., *A THz graphene metasurface for polarization selective virus sensing.* Carbon, (2021) 176: p. 580-591. available online:

https://www.sciencedirect.com/science/article/abs/pii/S0008622321002311

[13] H. Bi, M. Yang, and R. You, *Advances in terahertz metasurface graphene for biosensing and application.* Discover Nano, (2023) 18(1): p. 63. available online:

https://link.springer.com/article/10.1186/s11671-023-03814-8

[14] H. Liu, et al., *Coupled magnetic plasmons in metamaterials.* physica status solidi (b), (2009) 246(7): p. 1397-1406. available online:

https://onlinelibrary.wiley.com/doi/abs/10.1002/pssb.200844414

[15] N. Liu, S. Kaiser, and H. Giessen, *Magnetoinductive and electroinductive coupling in plasmonic metamaterial molecules.* Advanced Materials, (2008) 20(23): p. 4521-4525. available online:

https://onlinelibrary.wiley.com/doi/abs/10.1002/adma.200801917

[16] M. Fleischhauer, A. Imamoglu, and J.P. Marangos, *Electromagnetically induced transparency: Optics in coherent media.* Reviews of modern physics, (2005) 77(2): p. 633. available online: https://journals.aps.org/rmp/abstract/10.1103/RevModPhys.77.633

[17] C. Alzar, M. Martinez, and P. Nussenzveig, *Classical analog of electromagnetically induced transparency.* arXiv preprint quant-ph/0107061, (2001). available online: https://pubs.aip.org/aapt/ajp/article

abstract/70/1/37/1040315 / Classical-analog-of-electromagnetically-induced?redirectedFrom =fulltext

[18] É. Lheurette, *Classical Analog of Electromagnetically Induced Transparency*. Metamaterials and Wave Control, (2013) p. 195-214. available online:

https://onlinelibrary.wiley.com/doi/abs/10.1002/9781118762080.ch8

[19] S.E. Harris, *Electromagnetically induced transparency.* Physics today, (1997) 50(7): p. 36-42. available online: https://pubs.aip.org/physicstoday/article abstract/50/7/36/409812/Electromagnetically-Induced-TransparencyOne-can

[20] M. Servatkhah, and H. Alaei, *The Effect of Antenna Movement and Material Properties on Electromagnetically Induced Transparency in a Two-Dimensional Metamaterials.* Journal of Optoelectronical Nanostructures, (2016). 1(2): p. 31-38. available online: https://jopn.marvdasht.iau.ir/article_2046.html

[21] S. Taghipour, , G. Rezaei, and A. Gharaati, *Electromagnetically induced transparency in a spherical Gaussian quantum dot.* The European Physical Journal B, (2022) 95(9): p. 141. available online:

https://link.springer.com/article/10.1140/epjb/s10051-022-00409-7

[22] S. Ghafari, M.R. Forouzeshfard, and Z. Vafapour, *Thermo optical switching and sensing applications of an infrared metamaterial.* IEEE Sensors Journal, (2019) 20(6): p. 3235-3241. available online:

https://ieeexplore.ieee.org/abstract/document/8911485

[23] M.R. Nickpay, M. Danaie, and A. Shahzadi, *Highly sensitive THz refractive index sensor based on folded split-ring metamaterial graphene resonators.* Plasmonics, (2021) p. 1-12. available online:

https://link.springer.com/article/10.1007/s11468-021-01512-8

[24] S.A. Maier, *Plasmonics: fundamentals and applications*. Vol. 1. (2007) Springer. available online:

https://link.springer.com/book/10.1007/0-387-37825-1

[25] Zhang, S., et al., *Plasmon-induced transparency in metamaterials.* Physical review letters, (2008) 101(4): p. 047401. available online:

https://journals.aps.org/prl/abstract/10.1103/PhysRevLett.101.047401

[26] Z. Yi, , et al., *Dual-band plasmonic perfect absorber based on graphene metamaterials for refractive index sensing application.* Micromachines, (2019) 10(7): p. 443. available online: https://www.mdpi.com/2072-666X/10/7/443

[27] S. Khani, and M. Hayati, *Optical biosensors using plasmonic and photonic crystal band-gap structures for the detection of basal cell cancer.* Scientific reports, (2022) 12(1): p. 5246. available online:

https://www.nature.com/articles/s41598-022-09213-w

[28] M. Momeni, , M. Javadian Sarraf, and F. Khatib, *Design of high sensitivity and high FoM refractive index biosensor based on 2D-photonic crystal.* Journal of Optoelectronical Nanostructures,(2021). 6(4): p. 33-58. available online:

https://jopn.marvdasht.iau.ir/article_5040.html

[29] M.S.Z. Hosseini, A. Keshavarz, and A. Gharaati, *The effect of temperature on optical absorption cross section of bimetallic core-shell nano particles* (2016). available online: https://www.sid.ir/paper/349307/en

[30] Z.Vafapour, E.S. Lari, and M.R. Forouzeshfard, *Breast cancer detection capability of a tunable perfect semiconductor absorber: Analytical and numerical evaluation.* Optical Engineering, (2021). 60(10): p. 107101-107101. available online:

https://www.spiedigitallibrary.org/journals/optical-engineering /volume-60/issue-10/107101/Breast-cancer-detection-capability-of-a-tunable-perfect-semiconductor-absorber/10.1117/1.OE.60.10.107101.short

[31] A. Keshavarz, and Z. Vafapour, *Water-based terahertz metamaterial for skin cancer detection application.* IEEE Sensors Journal, (2018) 19(4): p. 1519-1524. available online: https://ieeexplore.ieee.org/abstract/document/8540886

[32] D. Li, , et al., *Identification of early-stage cervical cancer tissue using metamaterial terahertz biosensor with two resonant absorption frequencies.* IEEE Journal of Selected Topics in Quantum Electronics, (2021) 27(4): p. 1-7. available online: https://ieeexplore.ieee.org/abstract/document/9353192

[33] F. Wahaia, , et al., *Detection of colon cancer by terahertz techniques.* Journal of Molecular Structure, (2011) 1006(1-3): p. 77-82. available online:

https://www.sciencedirect.com/science/article/abs/pii/S0022286011004376

[34] A. Farmani, A. Mir, and H. Emami Nejad, *Numerical modeling of a metamaterial biosensor for cancer tissues detection.* Journal of Optoelectronical Nanostructures, (2020) 5(1): p. 1-18. available online: https://jopn.marvdasht.iau.ir/article_4030_526.html

[35] H. Fouladi, A. Farmani, and A. Mir, *Research Paper Rigorous Investigation of Ring Resonator Nanostructure for Biosensors applications in breast cancer detection.* Journal of Optoelectronical Nanostructures, (2023) 8(4): p. 97-119. available online:

https://jopn.marvdasht.iau.ir/article_6216_2941950397c94b88c91f81f6cee85910.pdf

[36] A. Hamouleh-Alipour, et al., *Blood hemoglobin concentration sensing by optical nano biosensor-based plasmonic metasurface: a feasibility study*. IEEE Transactions on Nanotechnology (2022) 21: p. 620-628. available online:

https://ieeexplore.ieee.org/abstract/document/9916145